Journal of the Oceanographical Society of Japan
Vol. 37, pp. 243 to 258, 1981

Statistical Characteristics of Individual Waves in Laboratory Wind Waves

I. Individual Wave Spectra and Similarity Structure*

Masayuki TOKUDA**† and Yoshiaki TOBA**

Abstract: Statistical characteristics of individual waves in laboratory wind waves have been studied by use of a wind-wave tunnel. The individual waves are defined by actual undulations of the water surface at any instant, and are characterized by concentrated shearing stress and strong vorticity at their crests. A conspicuous self-similarity structure is found in the individual wave field. The similarity manifests itself as a simple spectral form, and as the statistical 3/2-power law between nondimensional wave height and wave period, and further as the $-1/2$-power relationship between nondimensional phase speed and frequency, for waves of the high frequency side. The normalized energy spectrum, specially defined for individual waves, has a form practically equivalent to the traditional spectrum for component waves in the main frequency range from 0.7 to 1.5 in the frequency normalized by the peak frequency, but does not have secondary peaks at harmonics. The phase speed of individual waves also coincides with that of component waves in the main frequency range.

1. Introduction

Wind waves are the basic phenomena through which various phases of the interactions between the atmosphere and the ocean develop. However, many problems involving the phenomenon of wind waves are not yet fully understood physically. Quantitative treatment of the complicated phenomena of wind waves was initiated by SVERDRUP and MUNK (1947) who introduced the concept of significant waves. Since the concept of energy spectrum was introduced to the study of wind wave by PIERSON (1952) and NEUMAN (1952), a model of the wind-wave field that consists of freely traveling component waves has been widely accepted.

In the seventies, YEFIMOV *et al.* (1972), KATO and TSURUYA (1974) and RAMAMONJIARISOA (1974), reported that the dispersion relation of the linear wave theory was not satisfied by the one dimensional component waves of wind waves, and RIKIISHI (1978) reported that the dispersion relation also broke down for the two-dimensional component waves of laboratory wind waves. This has stimulated recent studies of strongly nonlinear wave models, in which the dominant waves are considered as the main carrier of wave energy, accompanied by their bound harmonics. LAKE *et al.* (1977), LAKE and YUEN (1978), MOLLO-CHRISTENSEN and RAMAMONJIARISOA (1978) proposed such models. MASUDA *et al.* (1979) and KUO *et al.* (1979) have shown that the peculiar behavior of the phase speed of the component waves may be explained mainly in terms of forced waves which have twice the frequency but travel with the same speeds as the dominant waves. The forced waves may be interpreted as a mathematical expression for the effect of the non-sinusoidal shape of the dominant waves, and the present article presents direct evidence of this.

Wind waves under direct action of the wind have many features very different from mere irregular wave trains mechanically generated on a water surface. First, the air flow over wind waves has a specific pattern with respect to the dominant individual waves, as brought to light by the studies of e.g. CHANG *et al.* (1971) and

* Received Jan. 5, revised Aug. 19 and accepted Nov. 24, 1981
** Geophysical Institute, Tohoku University, Sendai 980, Japan
† Present affiliation: Institute of Coastal Oceanography, National Research Center for Disaster Prevention, Science and Technology Agency, Hiratsuka 254, Japan

BANNER and MELVILLE (1976). In the present article, the term "individual waves" is used as expressing actual undulations of the water surface at any instant, in contrast to "component waves", which correspond to Fourier components of surface undulations. Secondly, there is the local wind drift caused by the shearing stress of the wind. BANNER and PHILLIPS (1974) and PHILLIPS and BANNER (1974) considered a shear flow at the surface to formulate the condition for wave breaking. Visualization of water flow near the surface has revealed unexpected features of wind waves. TOBA *et al.* (1975), OKUDA *et al.* (1976, 1977) and OKUDA (MS) have found that the shearing stress of the wind is concentrated at the crest and its windward face, consequently, extremely strong vorticity is concentrated near the crest, causing forced convection. This was partly reviewed by TOBA (1979). The traditional model of component waves regards the individual waves as a result of superposition of component free waves in random phases. However, the individual waves are accompanied by ordered motion other than the mere superposition of the orbital motion of irrotational component waves. These local distributions of stress and drift, air-flow separation (as studied by KAWAI, 1981) and wave breaking are all characteristics of individual waves under the action of the wind. There is a possibility that the mechanism of energy input from the wind to the wave is related to these near-surface phenomena that are associated with individual waves. In a wind-wave tunnel individual waves, though fluctuating, propagate for a considerable distance without losing their identity, while they are noticeably stretched in wavelength and amplified in wave height.

From the view point that this ordered motion may be represented by the individual waves, we will investigate the statistical characteristics of individual waves in the present paper. In particular, it will be shown below that the individual-wave field has a conspicuous self-similarity structure, and there are self-consistent relationships among their characteristics. As to the similarity structure, one of the authors (TOBA, 1972, 1978) already proposed a 3/2 power law between the nondimensional wave height and period of energy-containing waves and some associated relationships. TOBA (1978) proposed the concept of individual waves, pointing out that the 3/2 power law may be extended to individual waves, by use of some field data. The present experiments are a detailed investigation of this matter.

2. Experimental methods

The wind-wave tunnel used has a length of 8.10 m, a cross section of 0.15 m × 0.70 m and a water depth of 0.51 m, and is equipped with a multiblade fan at the head, and a permeable wave absorber at the end of the tank.

Experiments were performed for three wind conditions. For each wind condition, the wind profiles which were measured with a Pitot-static tube at three selected fetches of 1.70 m, 3.10 m and 5.45 m (Fetch Nos. 2, 4 and 7 in the lower part of Table 1) correlated well with the logarithmic form as shown in Fig. 1. Since the slopes of the profiles were similar to one an-

Table 1. Wind conditions and observation fetches.

Wind No.				U1		U2		U3
Mean friction velocity of air u_* (cm s^{-1})				46.4		67.8		102.0
Fetch No.	1	2	3	4	5	6	7	8
Fetch (m)	1.00	1.70	2.40	3.10	3.80	4.50	5.45	5.87

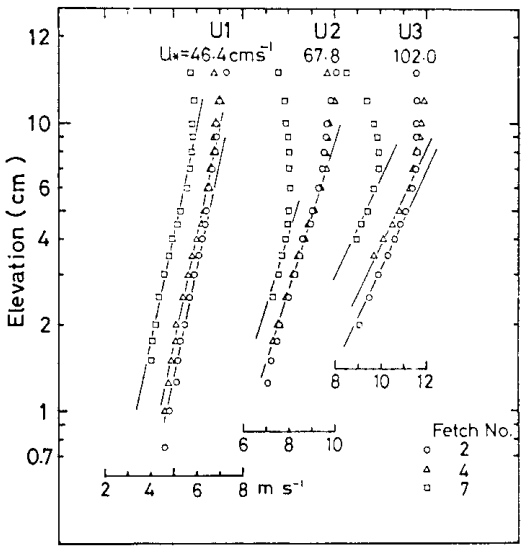

Fig. 1. Wind profiles for three wind conditions at three selected stations.

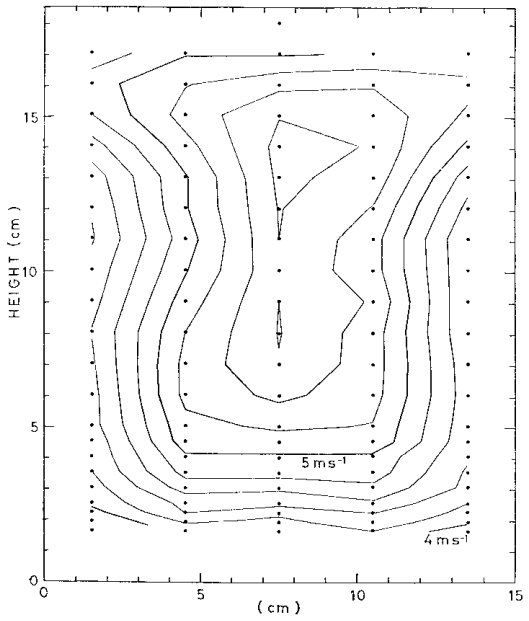

Fig. 2. An example of wind speed distribution in the cross section of the tunnel: Wind U1 at Fetch No. 8 (as in Table 1). The contours are drawn for every 0.2 m s^{-1}.

other for respective wind conditions, we adopted the mean friction velocity u_*, which was estimated from the mean slope of the profiles, as a measure of the respective wind conditions, and it is listed in the upper part of Table 1. We use Wind Numbers U1, U2 and U3 hereafter to represent the three wind conditions, whose u_* ranges from 46.4 cm s^{-1} (U1) to 102 cm s^{-1} (U3). Fig. 2 shows the wind speed distribution in the tunnel cross section at a fetch of 5.87 m (Fetch No. 8, Table 1) for the case of the Wind No. U1. It can be seen that the wind is nearly uniform laterally within 5 cm of the mean water level.

Wind generated waves were measured at eight fetches ranging from 1 m to 5.87 m (hereafter use Fetch Numbers 1 to 8 in the order of fetch as listed in the lower part of Table 1) by means of a pair of capacitance-type wave gauges placed Δl apart in the wind direction. The distance Δl was set within the range of 0.11- to 0.50-times (usually less than 0.3-times) the wave length of the spectral peak wave for each Fetch Number. A single pair of wave gauges was used for all Fetch Numbers successively on the basis of the assumption of stationarity of the wind wave field.

The traditional power and cross spectra were obtained as ensemble averages of 5 and 3 subsamples, respectively, for a frequency range up to 100 Hz with a resolution band width of 0.25 Hz. Each spectrum was smoothed using Hanning's spectral window. The time interval of sampling Δt was 0.02 s. Each sample consisted of 2048 data points (40.96 s).

3. Energy spectrum for individual waves

The individual waves are defined in the following two ways: zero-crossing trough-to-trough (ZCTT) and all trough-to-trough (ATT), as illustrated in Fig. 3(B) and (C), respectively. In the following discussion, however, analysis is made mainly of the ZCTT-type, and data are that of the ZCTT type analysis unless otherwise specified.

The power spectrum for individual waves has been defined and calculated according to the following procedure. Let Δt denote the sampling interval, and a region of frequency between zero and the Nyquist frequency $(2\Delta t)^{-1}$ is divided into n, then the resolution band width Δf is $\Delta f=(2n\Delta t)^{-1}$. Now, all the individual waves contained in the frequency band from f_i to $f_i+\Delta f$, the subscript i being 1 to n, are picked up from the wave gauge record of length τ_i, the number of waves m_i is counted, and the period $\tilde{T}_i^j$ and the wave height $\tilde{H}_i^j$ ($j=1, \cdots, m_i$) for each wave are determined according to the definition shown in Fig. 3(B) or 3(C). The mean period T_i and the mean height H_i are then determined by

$$T_i=\frac{1}{m_i}\sum_{j=1}^{m_i}\tilde{T}_i^j \quad \text{and} \quad H_i=\frac{1}{m_i}\sum_{j=1}^{m_i}\tilde{H}_i^j \qquad (3.1)$$

The spectral density of individual waves ϕ_i

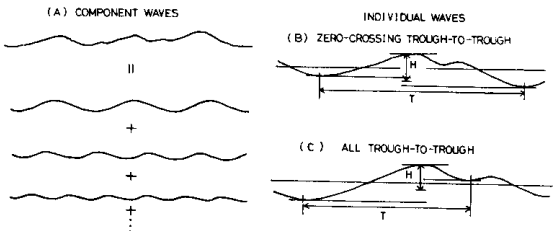

Fig. 3. Concept of component waves (A), and two types of individual waves: ZCTT-type (B), and ATT-type (C).

is defined for the frequency band f_i as

$$\phi_i \Delta f = \frac{1}{2} a_i^2 \quad (i=1,2,\ldots,n) \tag{3.2}$$

where a_i is the virtual mean amplitude defined by

$$a_i^2 = R_{m_i} (H_i/2)^2 \tag{3.3}$$

and where R_{m_i} is the rate of occupation or the proportion of time occupied by the waves of the i-th frequency band to the total length τ_t:

$$R_{m_i} = \frac{m_i T_i}{\tau_t} \tag{3.4}$$

Of course

$$\tau_t = \sum_{i=1}^{n} m_i T_i \tag{3.5}$$

where T_i is virtually equal to f_i^{-1}. In the present case, τ_t is around 204.8s, corresponding to five sub-samples. The concept of component waves is one of *superposition*, whereas the individual waves are *side-by-side*.

Regarding the spectrum as continuous, we omit the subscript i hereafter, and consider the energy density ϕ as a function of frequency f. It may be recognized that the energy density is the product of the rate of occupation and the squared wave height of individual waves in the respective frequency bands.

In order to compare the energy spectra of individual waves with those of the component waves, we use the normalized energy density. The normalization of the spectrum of component waves is made in the same way as HIDY and PLATE (1966) and MITSUYASU (1968):

$$\phi_N = f_p \phi / E, \quad E = \Sigma \phi \Delta f \tag{3.6}$$

where E is the total energy and f_p the frequency of the spectral peak.

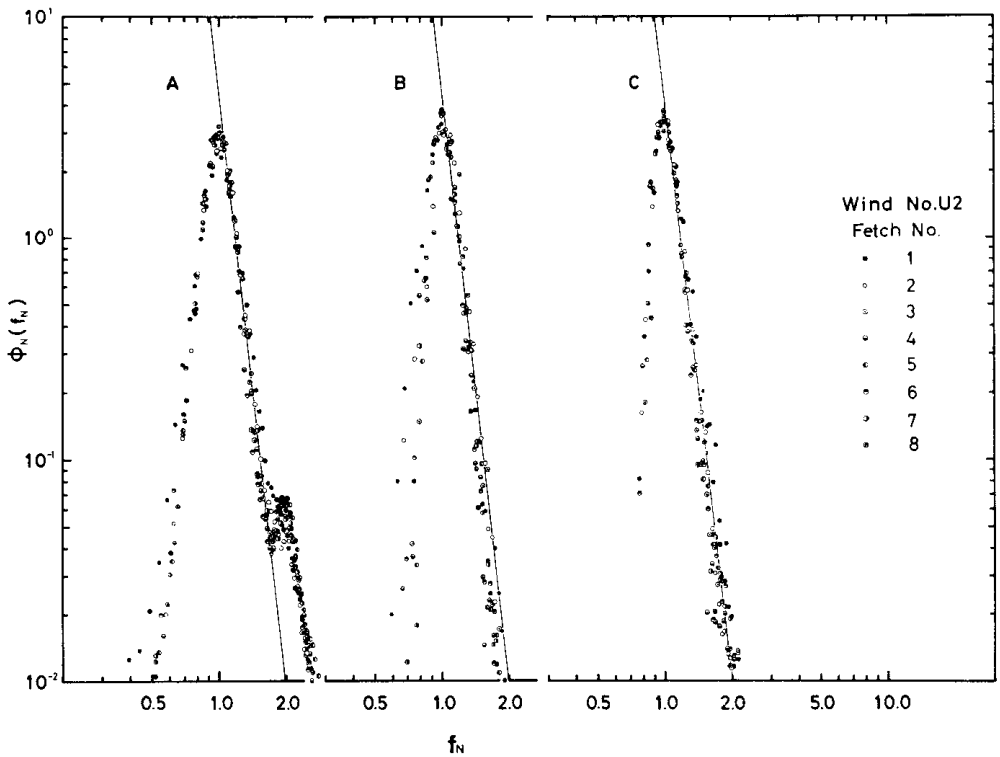

Fig. 4. Comparison of normalized energy spectra for the component waves and the individual waves. Data is shown for eight fetches in the case of Wind No. U2 ($u_*=67.8\,\mathrm{cm\,s^{-1}}$). A: Traditional energy spectra. B: Energy spectra for individual waves of ZCTT-type. C: Energy spectra for individual waves of ATT-type. Solid lines indicate the lower part of Eq. (3.10).

In the same way, the spectrum of individual waves is normalized as

$$\phi_N = R_{mN} H_N^2, \quad H_N = H/H_p \qquad (3.7)$$

where

$$R_{mN} = (H_p/\overline{H})^2 m_u f_N^{-1}, \; f_N = f/f_p, \; \overline{H} = (8E)^{1/2} \qquad (3.8)$$

and where

$$m_u = m/(\tau_t \Delta f) \qquad (3.9)$$

The subscripts N and p denote the normalized quantities and the ones corresponding to the spectral peak, respectively. The R_{mN} and $\overline{H}$ in (3.8) will be called the characteristic rate of occupation and the characteristic wave height, respectively. The above normalization makes the total energy of the spectrum equal to unity.

Fig. 4 shows the comparison among normalized spectra for component waves (A), individual waves of ZCTT-type (B) and those of ATT-type (C), for the case of Wind No. U2 ($u_*=67.8$ cm s^{-1}). From the figure, the following features may be pointed out. First, the distribution of ϕ_N is independent of the fetch for the case of individual waves, which corresponds with Mitsuyasu's (1968) report for component wave spectra. Secondly, $\phi_N \geqslant 0.1$, there is no practical difference between the component waves and the individual waves. However, the second peak of the former at $f_N=2$ is completely absent in the latter. The second peak of the spectrum (A) is interpreted as a manifestation of the distortion of the form of dominant individual wave from the sinusoidal form as first suggested by TOBA (1973), and it corresponds to the forced wave discussed by MASUDA *et al.* (1979). Thirdly, in the regions between the peak frequency and its first harmonics, the ATT-spectrum is in better agreement with the component wave spectrum than the ZCTT-spectrum is, whereas for the low frequency side of the peak, the ZCTT-spectrum is in better agreement. This is reasonable considering the definition of individual waves illustrated in Fig. 3. The form of the ATT-spectrum depends on the sensitivity of the wave gauge. If we are interested in individual waves of much

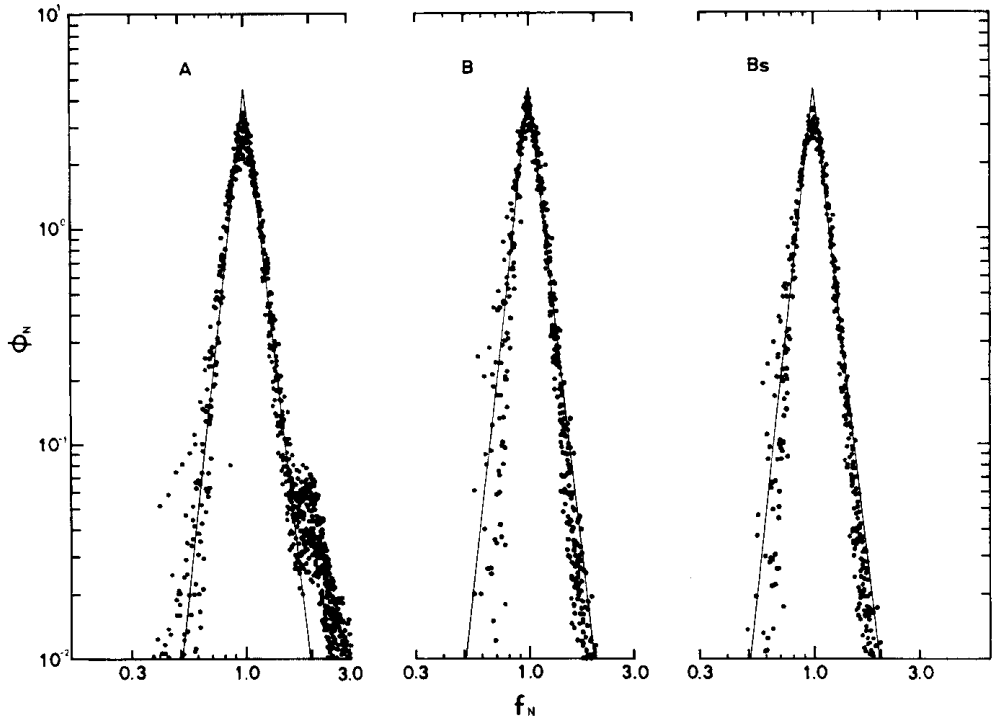

Fig. 5. As in Fig. 4 for A and B except it includes all wind conditions. B_s is a B-spectrum smoothed using Hanning's spectral window. Solid lines represent Eq. (3.10).

higher frequencies, we think that it is necessary to use a much more sensitive wave gauge, and make a stepwise extension of the ATT-spectra for several successive frequency bands up to the higher frequencies. In this case, a normalization using the peak spectral density will be more appropriate than (3.6) which is based on the total energy.

It has been ascertained that the above observations are applicable to all wind conditions, as shown in Fig. 5. Moreover, Fig. 5 shows that if the spectral density for the individual waves is smoothed using Hanning's spectral window because the data length is finite, the resulting spectrum shows better agreement with that of the component waves, especially in the vicinity of the spectral maximum.

For the region of higher energy density of $\phi_N \geqslant 0.1$, which corresponds to the normalized frequency range $0.7 < f_N < 1.5$, the effect of forced waves is negligible. We will call this range the main frequency range. Within this range, the normalized spectrum for the individual waves may be adequately approximated by the following simple forms,

$$\phi_N = \begin{cases} 4.4 f_N{}^{9} & \text{for } f_N < 1 \\ 4.4 f_N{}^{-9} & \text{for } f_N \geqslant 1 \end{cases} \qquad (3.10)$$

For wind waves in the ocean, the spectrum on the high frequency side of the main frequency range was formerly believed to be proportional to $g^2 f^{-5}$ as proposed by PHILLIPS (1958), while it has been pointed out by TOBA (1973), KAWAI *et al.* (1977) and TOBA (1978) that it should rather be proportional to $g u_* f^{-4}$, where g is the acceleration of gravity. For the case of our laboratory wind waves, the spectral form has a slope of $f^{\pm 9}$. Using data from a larger wind-wave tunnel, TOBA (1973) showed that the spectrum in the main frequency range had a slope of $f^{\pm 10}$, which is essentially the same as the present $f^{\pm 9}$. The dynamical reasons for the difference in spectral forms for the sea and for the laboratory tank are yet to be clarified.

The fact that the spectral form of the individual waves has a simple form as expressed by (3.10), independent of the fetch and the wind speed, strongly suggests that the individual waves in wind waves are controlled by some principle of similarity, presumably as a consequence of the strong nonlinearity inherent in wind-wave phenomena under the direct action of the wind.

Mathematical conversion from the newly defined individual wave spectra to the traditional component wave spectrum and vice versa is left for future study.

4. The 3/2-power law for individual waves and experimental details of the similarity

The upper part of Fig. 6 shows the wave height distribution with respect to the frequency, for Wind No. U2 ($u_* = 67.8$ cm s^{-1}). The existence of a kind of equilibrium range as to the height distribution which develops with the fetch is clear. The wave height in the equilibrium range may well be represented by a curve proportional to $f^{-3/2}$. To make this clearer, we make use of the following dimensionless forms,

$$H^* \equiv gH/u_*{}^2, \quad T^* \equiv gT/u_* \qquad (4.1)$$

For the significant wave height and period, TOBA (1972) already proposed the 3/2 power law,

$$H_G{}^* = B_G T_G{}^{*3/2} \qquad (4.2)$$

where the subscript G stands for significant waves. He has also shown that (4.2) may be extended statistically to individual waves of wind waves in the sea (TOBA, 1978). Fig. 7 represents, in dimensionless form, wave height in the upper part of Fig. 6, for comparison sake with (4.2). It is seen that the same law as (4.2) holds for the individual waves of frequencies greater than f_p, namely,

$$H^* = BT^{*3/2} \quad \text{for} \quad f \geqslant f_p \qquad (4.3)$$

especially in the main frequency range. The value of the universal constant B_G is 0.062 according to TOBA (1972) and 0.062 ± 0.010 according to KAWAI *et al.* (1977). In the case of individual waves in the laboratory, the value of B is smaller for shorter fetches and it attains a quasi-equilibrium value at Fetch No. 4 (3.10 m), expressed by

$$B = 0.043 \pm 0.002 \qquad (4.4)$$

where ± 0.002 is the standard deviation of the values listed in Table 2 for Fetch Nos. 5 to 8.

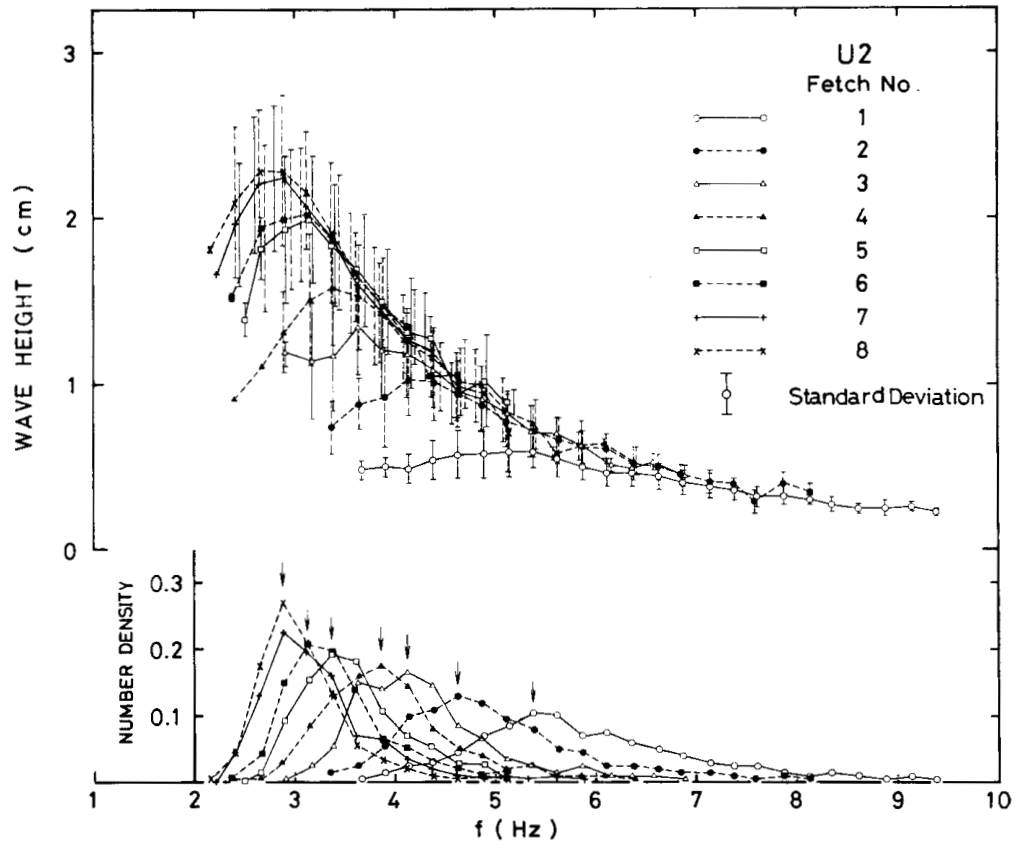

Fig. 6. Distributions of the wave height and the number density with respect to frequency for eight fetches for the case of U2 (u_*=67.8 cm s^{-1}). The arrows in the lower diagram indicate the peak frequency for each fetch.

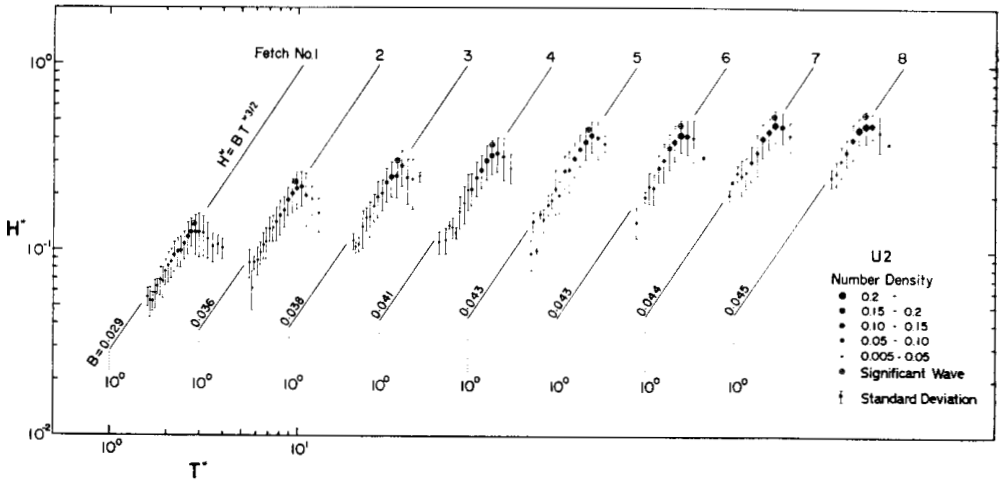

Fig. 7. Examples showing that the main part of the individual waves in the wind-wave tunnel satisfy the 3/2-power law of Eq. (4.3). The case of U2 (u_*=67.8 cm s^{-1}).

Table 2. Characteristic values for individual waves of the spectral peak.
H_p is determined from the wave record of the down stream gauge of the pair of wave gauges in the wind direction, and its location is indicated by the Fetch Number (as in Table 1). $\overline{H_p}$ indicates the mean wave height determined from the wave records of the pair of wave gauges. B is estimated from the best fit of the 3/2 power law to the observed distribution as shown in Fig. 7 on the high frequency side of the spectral peak, and B_p is determined from $B_p=H_p(gu_*)^{-1/2}T_p^{-3/2}$. δ_p is determined from $\delta_p=k_p\overline{H}_p/2\pi$.

Wind No. U1 ($u_*=46.4$ cm s^{-1}).

Fetch No.	1	2	3	4	5	6	7	8
σ_p (rad s^{-1})	44.4	38.5	30.8	26.9	25.6	23.1	21.4	20.4
k_p (rad cm^{-1})	1.188	0.931	0.635	0.515	0.451	0.378	0.343	0.322
C_p (cm s^{-1})	37.4	41.4	48.5	52.2	56.6	61.0	62.4	63.4
δ_p	0.0393	0.0565	0.0736	0.0746	0.0815	0.0757	0.0779	0.0766
H_p (cm)	0.18	0.37	0.71	0.97	1.09	1.30	1.49	1.51
$\overline{H}_p$ (cm)	0.21	0.38	0 73	0.91	1.14	1.26	1.42	1.49
B	0.017	0.027	0.036	0.041	0.043	0.045	0.045	0.045
B_p	0.016	0.026	0.036	0.040	0.042	0.043	0.044	0.042
E (cm^2)	4.03×10^{-3}	1.48×10^{-2}	5.33×10^{-2}	9.46×10^{-2}	1.23×10^{-1}	1.76×10^{-1}	2.21×10^{-1}	2.49×10^{-1}

Wind No. U2 ($u_*=67.8$ cm s^{-1}).

Fetch No.	1	2	3	4	5	6	7	8
σ_p (rad s^{-1})	33.6	27.5	24.3	22.7	20.4	19.7	18.1	18.0
k_p (rad cm^{-1})	0.675	0.480	0.377	0.336	0.270	0.254	0.223	0.220
C_p (cm s^{-1})	49.8	57.4	64.5	67.4	75.4	77.5	81.1	82.0
δ_p	0.0646	0.0807	0.0786	0.0803	0.0829	0.0821	0.0786	0.0782
H_p (cm)	0.59	1.01	1.20	1.53	1.99	2.02	2.24	2.28
$\overline{H}_p$ (cm)	0.60	1.06	1.31	1.49	1.93	2.03	2.20	2.24
B	0.029	0.036	0.038	0.041	0.043	0.043	0.044	0.045
B_p	0.028	0.036	0.035	0.041	0.045	0.043	0.043	0.043
E (cm^2)	3.67×10^{-2}	9.67×10^{-2}	1.65×10^{-1}	2.38×10^{-1}	3.61×10^{-1}	4.01×10^{-1}	4.93×10^{-1}	5.42×10^{-1}

Wind No. U3 ($u_*=102.0$ cm s^{-1}).

Fetch No.	1	2	3	4	5	6	7	8
σ_p (rad s^{-1})	23.6	22.5	19.4	18.0	16.6	16.6	16.1	15.3
k_p (rad cm^{-1})	0.360	0.333	0.242	0.209	0.173	0.173	0.167	0.157
C_p (cm s^{-1})	65.5	67.5	80.1	86.4	96.1	96.0	96.2	97.1
δ_p	0.0778	0.0860	0.0852	0.0896	0.0918	0.0900	0.0859	0.0923
H_p (cm)	1.31	1.67	2.29	2.62	3.32	3.44	3.41	3.73
$\overline{H}_p$ (cm)	1.34	1.62	2.19	2.68	3.32	3.25	3.22	3.67
B	0.032	0.036	0.040	0.041	0.046	0.046	0.045	0.046
B_p	0.030	0.036	0.039	0.040	0.045	0.047	0.044	0.045
E (cm^2)	1.63×10^{-1}	2.67×10^{-1}	5.29×10^{-1}	6.59×10^{-1}	1.07×10^{0}	1.17×10^{0}	1.18×10^{0}	1.45×10^{0}

The difference of the values of B_G and B is partially due to the fact that the significant wave height is always higher than the level of the height of individual waves.

Actually, the following relationships hold very well for our data,

$$T_G=T_P,\quad H_G=1.12\,H_P \qquad (4.5)$$

The value of B_G corresponding to (4.4) thus becomes 0.048, which is to some extent closer to 0.062. The variation of the value with fetch at shorter fetches will be discussed in Part II of the present series of papers on individual waves.

Fig. 8 shows the distribution of the normalized wave height H_N vs. f_N, revealing the applicability

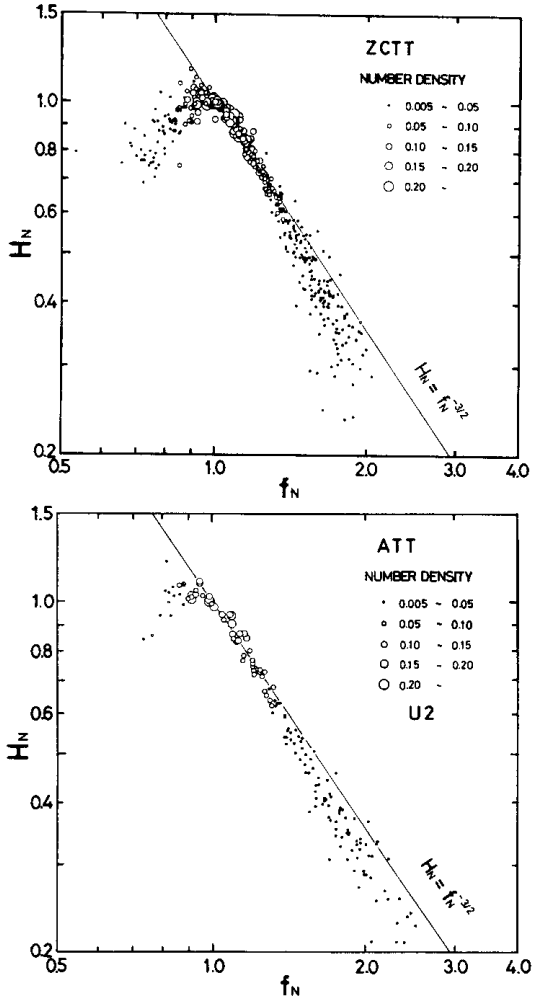

Fig. 8. Another representation of the 3/2-power law for individual waves of ZCTT-type for three wind conditions, and of ATT-type, for the case of U2 ($u_*=67.8\,\mathrm{cm\,s^{-1}}$). The solid lines indicate the lower part of Eq. (4.6).

of the 3/2-power law over the main frequency range on the high frequency side. This distribution can be approximated by

$$H_N=\begin{cases} f_N & \text{for } f_N<1 \\ f_N^{-3/2} & \text{for } f_N\geqslant 1 \end{cases} \qquad (4.6)$$

although for the range of $f_N<1$ the scattering of the points is rather large. Further, the relatively small number of individual waves for much higher frequencies deviate from this law. This range of large deviation, $f_N>1.5$, corresponds to the range where the -9 power law (3.10) deviates in Fig. 4.

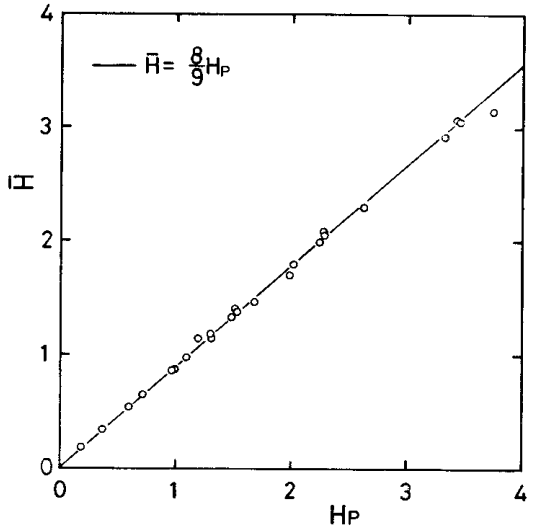

Fig. 9. Relation between the height of spectral peak wave H_p and the characteristic height $H=(8E)^{1/2}$ for three wind conditions. Solid line represents Eq. (4.7).

The lower part of Fig. 6 indicates the distribution of the number density of individual waves for the case of U2 ($u_*=67.8\,\mathrm{cm\,s^{-1}}$). It is seen that the frequency of the peak of the number density corresponds to that of the spectral maximum, and also that the number density has a similar distribution around the peak frequency. The similarity in the spectral form suggests that the ratio, $H_p/\bar{H}$, between the height of the peak wave and the characteristic height $(8E)^{1/2}$ is constant. This is supported by experimental results as shown in Fig. 9, giving

$$H_p/\bar{H}=9/8 \qquad (4.7)$$

Substituting (3.10), (4.6) and (4.7) in (3.7), the number distribution m_u, defined by (3.9), may be given by

$$m_u=\begin{cases} 3.5f_N{}^{8} & f_N<1 \\ 3.5f_N{}^{-5} & f_N\geqslant 1 \end{cases} \qquad (4.8)$$

This also has an experimental support as evidenced by Fig. 10.

From the figure, the following facts become clear. First, the normalized number distribution is independent of the fetch as well as of the wind speed. Second, the distribution has no second peak corresponding to the harmonics of the peak of component waves. Third, since

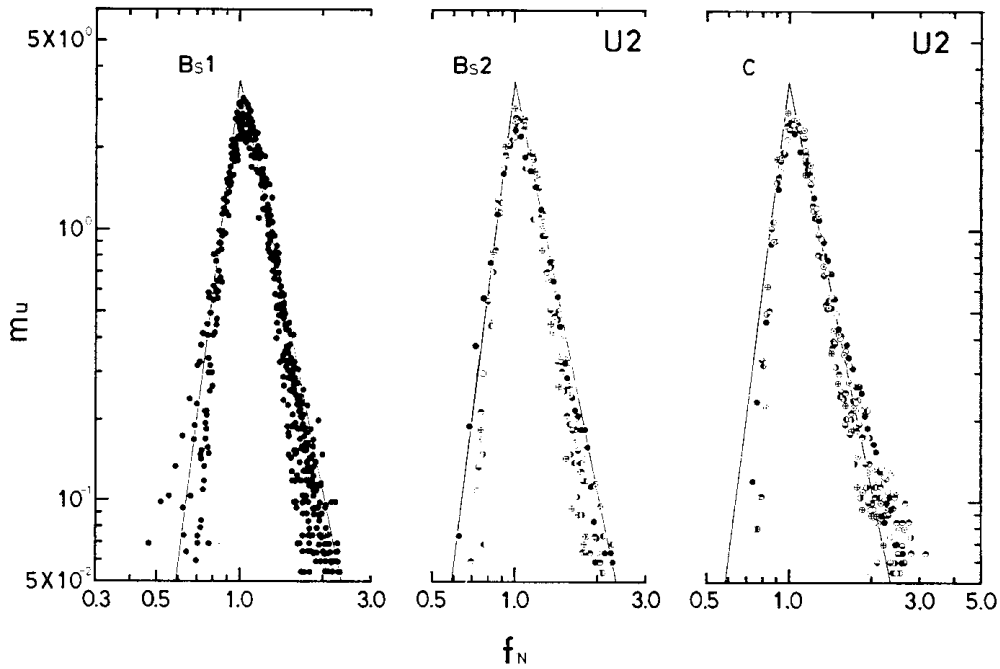

Fig. 10. Comparison of number distribution m_u of individual waves per unit scale of $\tau_t \Delta f$. B_s1: ZCTT-type for three wind conditions. B_s2: ZCTT-type for the case of U2 ($u_*=67.8\,\mathrm{cm\,s^{-1}}$). C: ATT-type for the case of U2. Solid lines represent Eq. (4.8). Different symbols stand for different fetches as in Fig. 4.

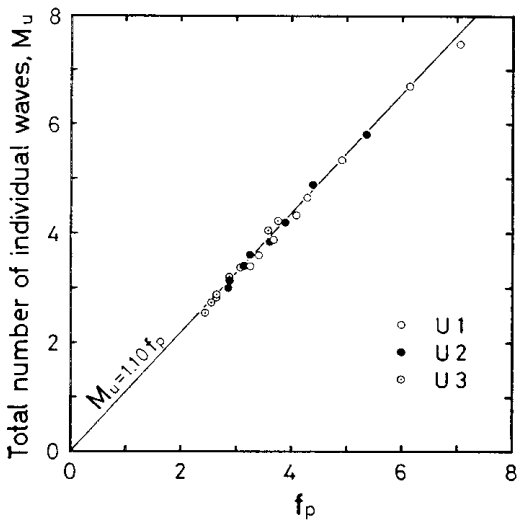

Fig. 11. Total number of individual waves per unit time versus the frequency of spectral peak wave for three wind conditions.

there is no large difference between the forms of H_N shown in the upper and the lower parts of Fig. 8 for ZCTT- and ATT-types, respectively, the difference between the energy spectra for the above two types of individual waves shown Fig. 4 is mostly a consequence of the difference in the number distribution. For a constant wind, the first fact mentioned above requires that the individual waves grow with the fetch without changing the normalized number distribution. This characteristic growth process is not easily expected from the standpoint of the traditional treatment of component waves. From (4.8), the total number M_u per unit time is expressed by

$$M_u=\int_0^\infty m_u df=f_p\int_0^\infty m_u df_N=1.3f_p \quad (4.9)$$

As shown in Fig. 11, (4.9) has good experimental support, except that the proportionality constant is 1.10. The discrepancy in the coefficient is mainly due to the disagreement of experimental values with (4.8) in the neighbourhood of $f_N=1$.

5. Experimental determination of phase speed and steepness of individual waves

The phase speed C of individual waves was

determined from records of a pair of wave gauges placed close to each other in the wind direction. We define C by $\Delta l/\Delta t$ where Δt is the time required for the center of the wave to travel the distance Δl between the pair of wave gauges. The center of an individual wave is represented here by the center of the points at which the wave record crosses the mean level. Since Δl used is smaller than 1/3 of the wave length of the spectral peak wave, except for cases of Fetch Nos. 1 (1.00 m) and 2 (1.70 m) for Wind No. U1 ($u_*=46.4\,\mathrm{cm\,s^{-1}}$), each individual wave can usually be identified easily on the pair of wave records. However, since the wave height and period determined in the two wave records are not exactly coincident, the average values are adopted as H and T. The phase speed of one-dimensional component waves was estimated from the cross spectra of the same records.

An example of phase speeds for individual waves and component waves is shown in Fig. 12 for Wind No. U2 ($u_*=67.8\,\mathrm{cm\,s^{-1}}$), Fetch No. 4 (3.10 m). In the region of high energy density in the vicinity of f_p, the two kinds of phase speed agree well with each other, although

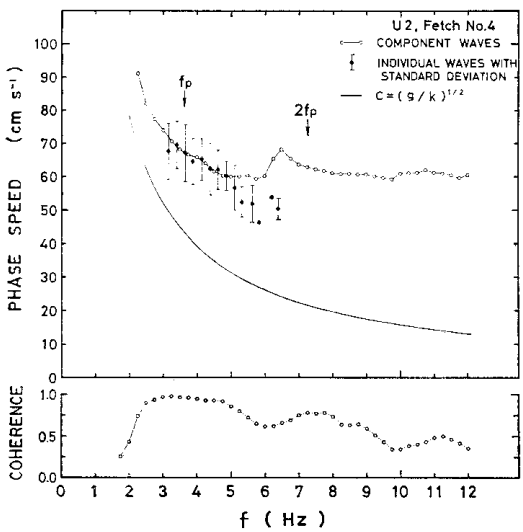

Fig. 12. An example of the comparison of phase speeds between the component waves determined from cross-spectra and the individual waves for ZCTT-type at Fetch No. 4 (3.10 m) for the case of U2 ($u_*=67.8\,\mathrm{cm\,s^{-1}}$). The point without standard deviation indicates that the number of individual wave was only one. The coherence of the cross-spectra is shown at the bottom.

these values are considerably greater than the value estimated from linear theory, which is shown by a thin curve.

While the phase speed of individual waves has a distribution which decreases with the frequency, that of the component waves tends to be nearly constant, in a similar manner to the results reported by RAMAMONJIARISOA (1974), for frequencies above 1.4 f_p. This is explained as being a consequence of the influence of the bound harmonics, or the shape effect of energy containing waves as already indicated in the spectral distribution. Close inspection shows that the phase speed of component waves in the vicinity of $2f_p$ seems to repeat the value found in the vicinity of f_p, and at higher frequencies it is eventually constant. MITSUYASU *et al.* (1979) have recently explained these characteristics of component wave phase speed in terms of forced waves, namely, bound harmonics of energy containing waves, by use of random gravity waves free from the wind.

In the main frequency range, where the phase speeds of component waves and individual waves coincide with each other, the coherence of the cross-spectra is close to unity. COX (1958) pointed out using a wind-wave experiment that when the distance between the pair of wave gauges becomes large compared to the wave

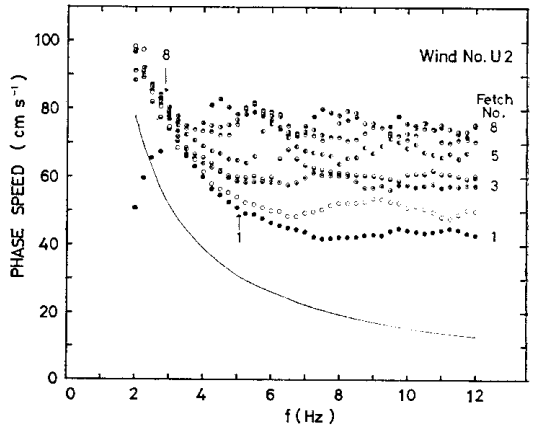

Fig. 13. Original values of the phase speed distribution for the component waves, for eight fetches for the case of U2 ($u_*=67.8\,\mathrm{cm\,s^{-1}}$), before the normalization shown in Fig. 15. Peak frequencies for Fetch Nos. 1 (1.00 m) and 8 (5.87 m) are indicated by arrows, other cases lie between these. The phase speed of linear water waves is shown by the full line.

length, the coherence becomes small, and the obtained component wave phase speed becomes unreliable. In our experiment, however, since Δl used was usually 0.1- to 0.3-times the wave length of the spectral peak wave, our measurement of the phase speed in the main frequency range f_N from 0.7 to 1.5 is considered reliable, and is of course reliable for that of individual

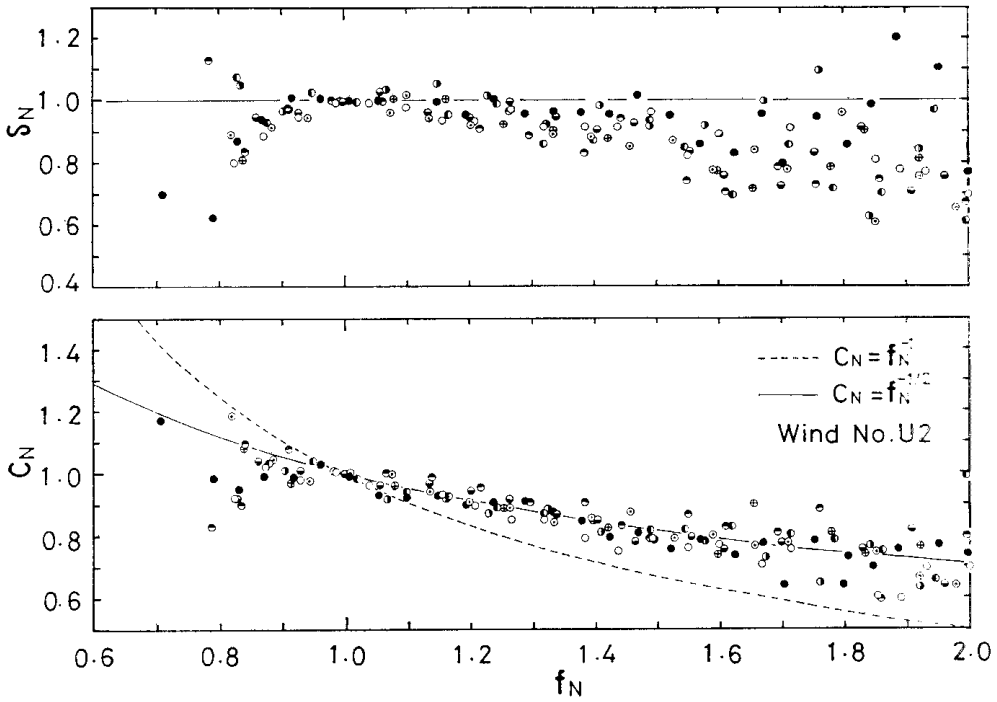

Fig. 14. Normalized wave steepness and phase speed of individual waves as a function of normalized frequency for the case of U2 (u_*=67.8 cm s^{-1}). The dispersion relation for linear water waves is also shown by the dotted line in the lower diagram.

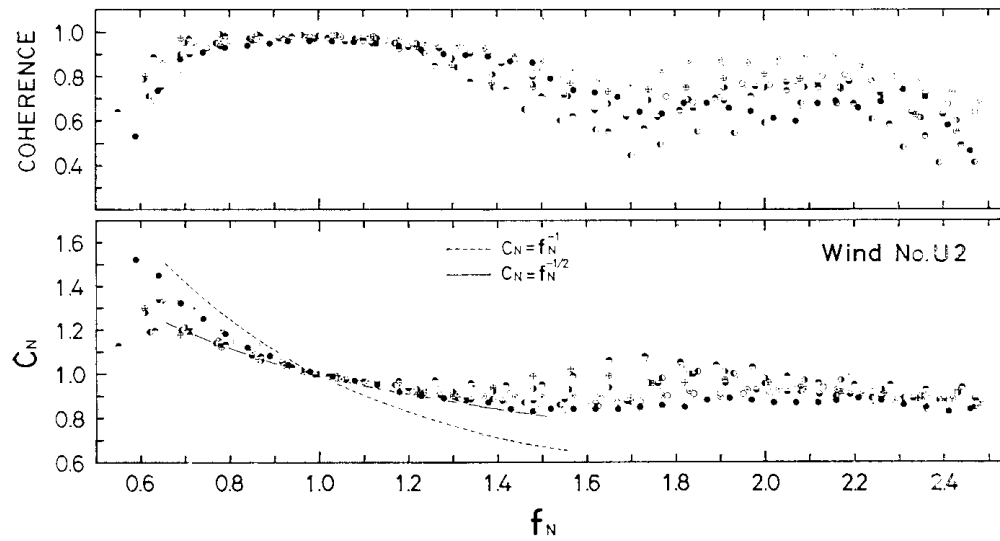

Fig. 15. Normalized phase speed of component waves as a function of normalized frequency for the same case as Fig. 14. The coherence of the cross-spectra is shown in the upper part.

waves.

Fig. 13 shows the phase speed data for component waves at each fetch for the case of Wind No. U2 ($u_*=67.8$ cm s^{-1}). The overall shape of the curve is the same as Fig. 12, but the value increases as the energy containing waves develop with the fetch.

The phase speed has now tentatively been normalized by that of the peak wave, and it is shown in Fig. 14 for individual waves and in Fig. 15 for the component waves, respectively, for all fetches in the case of U2 ($u_*=67.8$ cm s^{-1}). The normalized phase speed distribution is largely independent of the fetch, in the main frequency range for both kinds of waves, and is approximated by

$$C_N=f_N^{-1/2}=\sigma_N^{-1/2}, \quad \text{for} \quad f_N\geqslant 1 \qquad (5.1)$$

where $\sigma_N=\sigma/\sigma_P$ and $\sigma=2\pi f$. This is different from the dispersion relation predicted by the linear theory. The above item is also applicable to the other two wind conditions. A possible explanation of these experimental results will be given in part II.

From the determined phase speed C and the period T, we may obtain the wavelength λ and the wave number k for each individual wave by

$$\lambda=CT \quad \text{and} \quad k=2\pi/\lambda \qquad (5.2)$$

The lower part of Fig. 16 shows C_N for the individual waves as a function of the normalized wave number $k_N=k/k_P$, instead of f_N. An approximate relation obtained from the figure is

$$C_N=k_N^{-1/3} \qquad (5.3)$$

From (5.1) and (5.3), it follows that

$$\sigma_N=k_N^{2/3} \qquad (5.4)$$

The experimental support for (5.4) is shown in Fig. 17.

The steepness of the individual waves δ may be determined from H and k of (5.2) by the definition

$$\delta=kH/2\pi \qquad (5.5)$$

It should be noticed that this steepness is one derived from the observed H, C and T, and it should clearly be distinguished from that estimated from H and σ by use of the linear theory. The upper parts of Figs. 14 and 16 show the

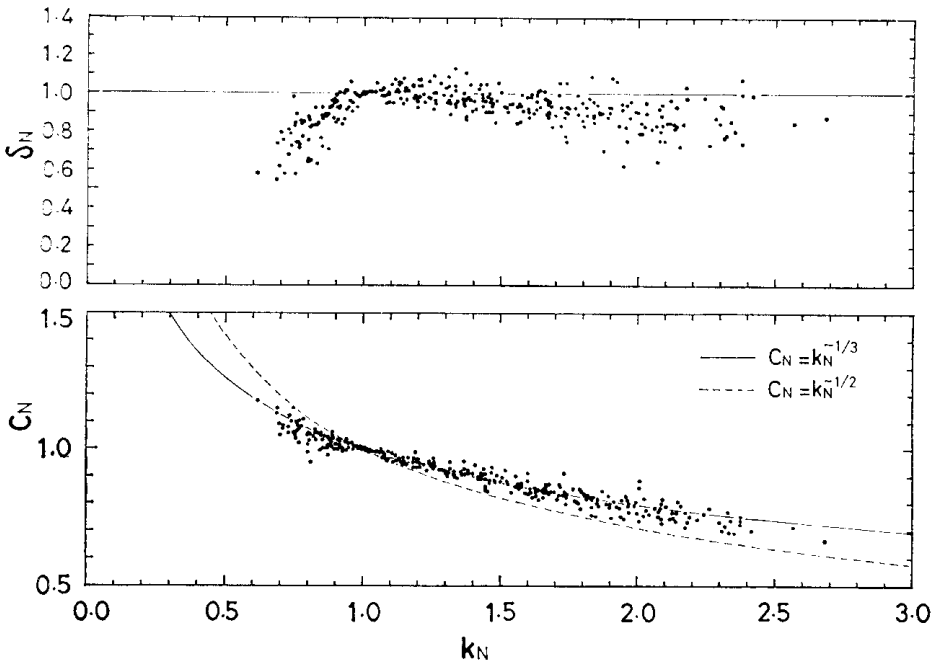

Fig. 16. Distributions of normalized wave steepness and phase speed of individual waves as a function of normalized wave number for three wind conditions. In the lower part, the dispersion relation for linear water waves is also shown by the dotted line.

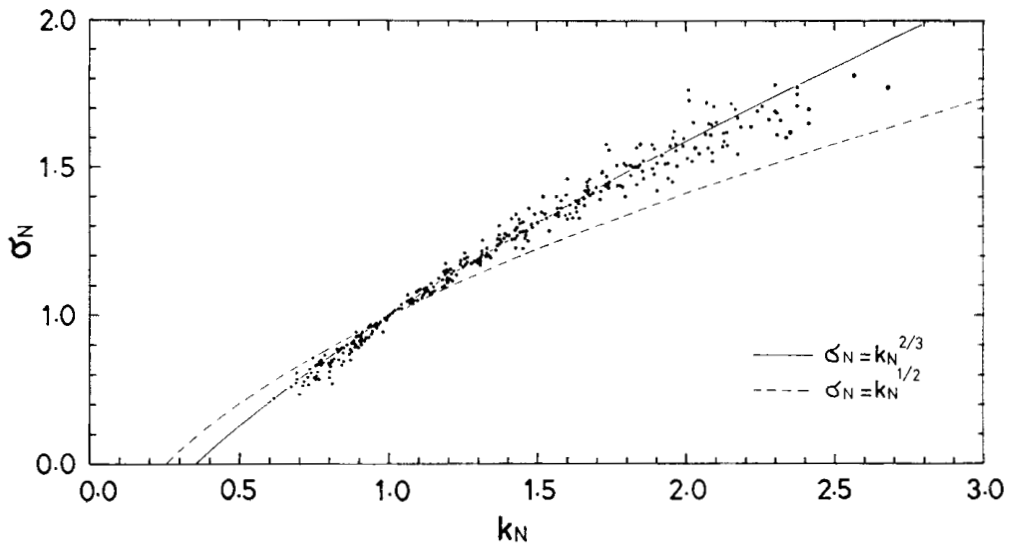

Fig. 17. Approximated dispersion relation of individual waves in the wind-wave tunnel. The dotted line shows the dispersion relation for linear water waves.

normalized steepness $\delta_N=\delta/\delta_P$. The figures show that the normalized steepness is around unity in the main frequency range on the high frequency side, namely,

$$\delta_N \approx 1 \quad \text{for} \quad f_N \geqslant 1 \tag{5.6}$$

This normalized wave steepness can be obtained by a combination of the 3/2 power law (4.6) and the normalized dispersion relation (5.4). Consequently, these three relationships are self-consistent with one other. A more detailed discussion regarding these self-consistent relationships will be given in Part II.

Finally, in relation to the 3rd paragraph of this section, we examine to what extent the form of the peak wave is close to that of Stokes waves. The presence of the bound harmonics of the peak wave in the high frequency range of the spectral density distribution for the component waves was already shown in Fig. 4. The form of Stokes wave up to the 3rd order is given by

$$\eta=a\cos kx+\frac{1}{2}ka^2\cos 2kx+\frac{3}{8}k^2a^3\cos 3kx \tag{5.7}$$

and the steepness δ is expressed by

$$\pi\delta=ka+\frac{3}{8}(ka)^3 \tag{5.8}$$

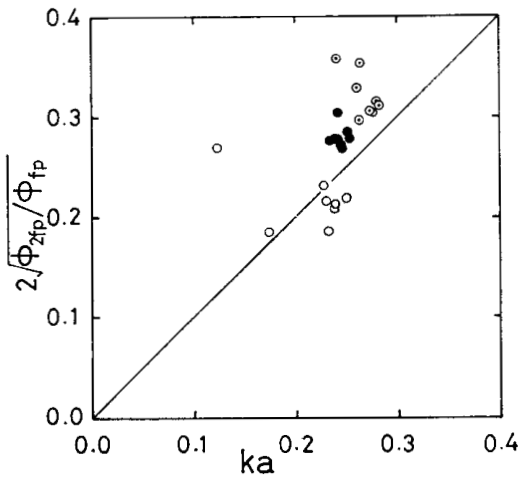

Fig. 18. Twice squared ratio of the spectral densities of the second harmonics and the peak wave component plotted against peak wave steepness. The straight line represents Eq. (5.9) which corresponds to Stokes waves. Different symbols stand for three wind numbers as in Fig. 11.

The ratio of the spectral densities, for constant bandwidth, of the second harmonics and the peak waves ϕ_{2fr}/ϕ_{fp} for Stokes waves should be expressed by use of k and a from (5.7) as

$$\phi_{2fp}/\phi_{fp}=(1/4)(ka)^2 \tag{5.9}$$

On the other hand, the value of ϕ_{2fp}/ϕ_{fp} for actual individual waves may be estimated from

the spectral distribution of component waves, and the value of a is obtained from δ by (5.8). The observed values of $2\sqrt{\phi_{2fp}/\phi_{fp}}$ for component waves are compared with the straight line for Stokes waves in Fig. 18. There is some deviation. However, we may interpret it in an approximate sense, and say that the irrotational part of the motion of the individual waves may be represented by Stokes waves, and this corresponds to the concept of forced waves described by MASUDA *et al.* (1979).

Acknowledgements

The authors wish to express many thanks to the members of our Physical Oceanography Laboratory, Tohoku University, especially, Dr. S. KAWAI, Dr. K. OKUDA, Messrs M. HATORI, Y. IMAI, Drs. P.S. JOSEPH, M. KOGA, Messrs. K. HANAWA, H. KAWAMURA and Miss Y. INOHANA, for helpful discussion and/or collaboration in various phases of this work. The authors also thank the reviewers for valuable comments for the revision of the paper. This study was partially supported by the Grant-in-Aid for Scientific Research by the Japanese Ministry of Education, Science and Culture, Project Nos. 374020 and 374123.

References

BANNER, M.L. and O.M. PHILLIPS (1974): On the incipient breaking of small scale waves. J. Fluid Mech., **65**, 647-656.

BANNER, M.L. and W.K. MELVILLE (1976): On the separation of air flow over water waves. J. Fluid Mech., **77**, 825-842.

CHANG, P.C., E.J. PLATE and G.M. HIDY (1971): Turbulent air flow over the dominant component of wind-generated water waves. J. Fluid Mech., **47**, 183-208.

COX, C.S. (1958): Measurements of slopes of high-frequency wind waves. J. Mar. Res. **16**, 199-225.

HIDY, G.M. and E.J. PLATE (1965): Wind action on water standing in a laboratory channel. J. Fluid Mech., **26**, 651-687.

KATO, H. and K. TSURUYA (1974): On the phase velocity of component waves of wind waves (in Japanese). Proc. 21st Japanese Conf. Coast. Eng., 255-259.

KAWAI, S. (1981): Visualization of air-flow separation over wind-wave crests under moderate wind. Boundary-Layer Meteorol., **21**, 93-104.

KAWAI, S., K. OKADA and Y. TOBA (1977): Support of the three-seconds power law and the $gu_*\sigma^{-4}$-spectral form for growing wind waves with field observational data. J. Oceanogr. Soc. Japan, **33**, 137-150.

KUO, Y.Y., H. MITSUYASU and A. MASUDA (1979): Experimental study on the phase velocity of wind waves. Part 1. Laboratory wind waves. Rep. Res. Inst. Appl. Mech., Kyushu Univ., **27**, 1-19.

LAKE, B., H. YUEN, H. RUNGALDIER and W. FERGUSON (1977): Nonlinear deep-water waves: theory and experiment. Part 2. Evolution of a continuous wave train. J. Fluid Mech., **83**, 49-74.

LAKE, B. and H. YUEN (1978): A new model for nonlinear wind waves. Part 1. Physical model and experimental evidence. J. Fluid Mech., **88**, 33-62.

MASUDA, A., KUO, Y.Y. and H. MITSUYASU (1979): On the dispersion relation of random gravity waves. Part 1. Theoretical framework. J. Fluid Mech., **92**, 717-730.

MITSUYASU, H., Y.Y. KUO and A. MASUDA (1979): On the dispersion relation of random gravity waves. Part 2. An experiment. J. Fluid Mech., **92**, 731-749.

MOLLO-CHRISTENSEN and A. RAMAMONJIARISOA (1978): Modelling the presence of wave groups in a random wave field. J. Geoph. Res., **83**, 4117-4122.

NEUMANN, G. (1952): On wind generated ocean waves with special reference to the problem of wave forecasting. Dept. Met. and Oceanogr., New York Univ. Prepared for Office of Naval Res., 136 pp.

OKUDA, K. (MS): Internal flow structure of short wind waves. Parts I, II and III. Submitted to J. Oceanogr. Soc. Japan.

OKUDA, K., S. KAWAI, M. TOKUDA and Y. TOBA (1976): Detailed observation of the wind-exerted surface flow by use of flow visualization method. J. Oceanogr. Soc. Japan, **32**, 51-62.

OKUDA, K., S. KAWAI and Y. TOBA (1977): Measurement of skin friction distribution along the surface of wind waves. J. Oceanogr. Soc. Japan, **33**, 190-198.

PHILLIPS, O.M. (1958): The equilibrium range in the spectrum of wind-generated waves. J. Fluid Mech., **4**, 426-434.

PHILLIPS, O.M. and M.L. BANNER (1974): Wave breaking in the presence of wind drift and swell. J. Fluid Mech., **66**, 625-640.

PIERSON, W.J., JR. (1952): A unified mathematical theory for the analysis, propagation and refraction of storm generated ocean surface waves. Parts I and II. Dept. Met. and Oceanogr., New York Univ. Prepared for Beach Erosion Board and Office of Naval Res., 461 pp.

RAMAMONJIARISOA, A. (1974): Contribution à l'étude de la structure statistique et des mécanismes de génération des vagues de vent. Thèse à L'Université de Provence (Inst. Méch. Stat. de la Turbulence, No. A.O. 10023), 160 pp.

RIKIISHI, K. (1978): A new method for measuring the directional wave spectrum. Part II. Measurement of the directional spectrum and phase velocity of laboratory wind waves. J. Phys. Oceanogr., **8**, 519-529.

SVERDRUP, H. U. and W. H. MUNK (1947): Wind, sea and swell: Theory of relations for forecasting. U. S. Navy Hydrogr. Office, Wash., Pub. No. 601, 44 pp.

TOBA, Y. (1972): Local balance in the air-sea boundary processes. I. On the growth process of wind waves. J. Oceanogr. Soc. Japan, **28**, 108-120.

TOBA, Y. (1973): Local balance in the air-sea boundary processes. III. On the spectrum of wind waves. J. Oceanogr. Soc. Japan, **29**, 209-220.

TOBA, Y. (1978): Stochastic form of the growth of wind waves in a single parameter representation with physical implications. J. Phys. Oceanogr., **8**, 494-507.

TOBA, Y. (1979): Study on wind waves as a strongly nonlinear phenomenon. Twelfth Symp. on Naval Hydrodyn., Nat. Acad. of Sci., Wash., D. C., 529-540.

TOBA, Y., M. TOKUDA, K. OKUDA and S. KAWAI (1975): Forced convection accompanying wind waves. J. Oceanogr. Soc. Japan, **31**, 192-198.

YEFIMOV, V. V., YU P. SOLOV'YEV and G. N. KHRISTOFOROV (1972): Observational determination of the phase velocities of spectral components of wind waves. Izv., Atmos. Ocean. Phys., **8**, 246-251.

実験室の風波における個々波の統計的な特性

I. 個々波のスペクトルと相似構造

徳 田 正 幸*†, 鳥 羽 良 明*

要旨: 瞬間瞬間の水面の実際の起伏によって定義される個々波を用いて，実験室の風波の場の統計的特性を研究した．この個々波は，峰に集中した接線応力と強い渦度領域で特徴づけられるものである．個々波解析による風波の統計的特性として，新しく定義したパワースペクトル，波高分布，個数分布，位相速度分布そして波形勾配分布を求めたが，個々波の場に顕著な自己相似構造があることが見いだされた．この相似性は，単純なスペクトルの形と，高周波側における無次元波高と周期の間の3/2乗則や，無次元位相速度と周期の間のマイナス1/2乗の関係として表われている．これらの分布を伝統的な成分波による結果と比較したところ，規格化された個々波のパワースペクトル分布は，ピーク周波数で規格化された周波数の0.7ないし1.5の主要周波数領域で，成分波のスペクトルと実質的に同等の形をもつが，ピーク波の高調波に成分波で見られる2次的なピークをもっていないこと，また規格化された位相速度分布においても，両者は主要周波数領域でよく一致することが示された．

* 東北大学理学部: 〒980 仙台市荒巻字青葉
† 現在国立防災科学技術センター平塚支所:
〒254 平塚市虹ケ浜9-2